

Phonons in few-layer graphene and interplanar interaction: A first-principles studySrijan Kumar Saha,^{1,2} U. V. Waghmare,³ H. R. Krishnamurthy,^{1,2} and A. K. Sood¹¹*Department of Physics, Indian Institute of Science, Bangalore 560012, India*²*Condensed Matter Theory Unit, Jawaharlal Nehru Centre for Advanced Scientific Research, Bangalore 560064, India*³*Theoretical Sciences Unit, Jawaharlal Nehru Centre for Advanced Scientific Research, Bangalore 560064, India*

(Received 27 June 2008; revised manuscript received 10 September 2008; published 24 October 2008)

We use first-principles density-functional theory calculations to determine the vibrational properties of ultrathin $n(1, 2, \dots, 7)$ -layer graphene films and present a detailed analysis of their zone-center phonons. We demonstrate that a low-frequency ($\sim 112 \text{ cm}^{-1}$) optical phonon with out-of-plane displacements exhibits a particularly large sensitivity to the number of layers, although no discernible change in the interlayer spacing is found as n varies. Frequency shifts of the optical phonons in bilayer graphene are also calculated as a function of its interlayer separation and interpreted in terms of the interplanar interaction.

DOI: [10.1103/PhysRevB.78.165421](https://doi.org/10.1103/PhysRevB.78.165421)

PACS number(s): 81.05.Uw, 71.15.Mb, 63.20.-e, 78.30.-j

I. INTRODUCTION

Recently, thanks to advances in the fabrication and manipulation of ultrathin multilayer graphene films, a lot of attention has been devoted to the study of how the physics of multilayer graphene evolves with increasing number of layers.¹⁻¹² Exciting theoretical and experimental work has been reported on the electronic properties of $n(>1)$ -layer graphene (n LG), addressing the effects of interlayer interaction, stacking order,³ orientational disorder,^{10,11} and external electric field.¹² The first experimental study¹ of electronic transport in n LG films determined the nature of their charge carriers and revealed a strong ambipolar electric-field effect. Subsequently, density-functional calculations³ which examined the dependence of their electronic band structure on the stacking order and the number of layers have shown that the observed ambipolar transport is only possible in Bernal (AB)-stacked n LG films. Furthermore, *ab initio*³ and tight-binding⁹ calculations as well as experimental studies¹¹ have made it clear that the Dirac-type linear dispersion present in (single-layer) graphene is also present in any AA -stacked n LG in graphene films with misoriented layers and in AB -stacked graphene films with odd number of layers.

While there are many studies on the electronic structure of the n LG films, their vibrational properties have not been fully explored. In particular, it is presently unclear how the out-of-plane vibrations are affected by the interlayer interaction and the number of layers. A quantitative understanding of these issues is crucial for the optical probing of futuristic graphene based nanoelectronic devices. In this paper, we calculate the vibrational properties of ultrathin n -layer graphene films (for $n=1, 2, \dots, 7$) using *ab initio* density-functional theory (DFT). We show that a low-frequency zone-center optical phonon with out-of-plane displacements is highly sensitive to the number of layers. A detailed analysis of all the phonon modes at the high-symmetry zone-center (Γ) point is also presented.¹³

The paper is organized as follows. In Sec. II, we briefly describe the technical aspects of our first-principles calculations. Section III presents the results (including structural relaxations, phonons, mode symmetries, and optical activities) for bulk graphite, single-layer graphene, and ultrathin

n -layer graphene films. In Sec. IV, we discuss the underlying physics of our main results together with the pictorial representation of the phonon modes. Finally, Sec. V contains some concluding remarks.

II. METHODOLOGY

All our calculations are performed using the PWSCF (Ref. 14) implementation of DFT, with a plane-wave basis set and ultrasoft pseudopotentials.¹⁵ We adopt the exchange-correlation functional of Perdew-Zunger (PZ) (Ref. 16) for the local-density approximation (LDA) and that of Perdew-Burke-Ernzerhof (PBE) (Ref. 17) for the generalized gradient approximation (GGA). The n LG films are simulated using a supercell geometry with a vacuum of 10 \AA in the z direction to ensure negligible interaction between its periodic images. The Brillouin-zone integration is done on uniform Monkhorst-Pack¹⁸ grids of $72 \times 72 \times 1$ for monolayer graphene, $72 \times 72 \times 3$ for few-layer graphene, and $72 \times 72 \times 24$ for bulk graphite. An electronic smearing parameter¹⁹ of 0.01 Ry with Fermi-Dirac distribution is used. Structural relaxation is carried out in each case so as to minimize the forces acting on each of the atoms using the Broyden-Fletcher-Goldfarb-Shanno (BFGS) based method.²⁰ Phonon frequencies are obtained using the density-functional perturbation theory (DFPT) (Ref. 21) which calculates full dynamical matrices through the linear response of electrons to a static perturbation induced by the ionic displacements.

III. RESULTS AND ANALYSIS

For sparsely layered systems such as graphite, with predominantly van der Waals interlayer interactions, standard DFT based approaches such as LDA and GGA are known to yield poor predictions for interlayer spacings.^{22,23} However, in case of graphite, LDA fortuitously gives reasonable interlayer spacing while GGA shows no binding at the measured spacing.^{3,24-26} Our LDA estimates of the equilibrium in-plane lattice spacing ($a_0^{\text{LDA}} = 2.4394 \text{ \AA}$) and interlayer distance ($d_0^{\text{LDA}} = 3.2932 \text{ \AA}$) of AB -stacked graphite are close to the respective experimental²⁷ values $a_0^{\text{expt}} = 2.46 \text{ \AA}$ and $d_0^{\text{expt}} = 3.35 \text{ \AA}$. While the GGA can reproduce the experimental

TABLE I. Optical phonons of 3D graphite and two-dimensional (2D) monolayer graphene at the high-symmetry point Γ . The meaning of “primed” is discussed in the text. The notations LO and TO are with respect to in-plane phonon wave vector $\mathbf{q} \rightarrow \mathbf{0}$.

Symmetry	Activity	Description	Frequency of graphite (cm ⁻¹)				Frequency of graphene (cm ⁻¹)
			GGA fully theoretical	GGA with d_0^{expt}	LDA fully theoretical	Experiment	LDA
$E_{2g}(\text{low})$ ^a	Raman	In-plane optical, primed (iLO'/TO')	8.9	49.3	53.7	49 ^b , 42 ^c	
$B_{2g}(\text{low})$	Silent	Out-of-plane optical, primed (oTO')	29.1	134.6	112.1	95 ^d , 126 ^c	
$B_{2g}(\text{high})$	Silent	Out-of-plane optical (oTO)	880.2	875.3	894.0	868 ^c	
$A_{2u}(\text{high})$	IR	Out-of-plane optical (oTO)	880.4	879.6	902.2	870 ^c	907.0
$E_{2g}(\text{high})$ ^a	Raman	In-plane optical (iLO/TO)	1560.6	1559.5	1594.1	1582 ^c	1593.9
$E_{1u}(\text{high})$ ^a	IR	In-plane optical (iLO/TO)	1561.6	1566.5	1601.4	1588 ^c	

^aDoubly degenerate phonon.

^bReference 28.

^cReference 29.

^dReference 30.

a_0 , it gives too large d_0 (4.2415 Å). Hence, for the GGA, phonon frequencies have been calculated for the theoretical as well as for the experimental d_0 ; while the former strongly underestimates the low-frequency modes, the latter improves the agreement with experiments but generates an unwanted c -axis pressure of 3.2 GPa. To obtain converged results, low-frequency phonons require relatively larger values of cutoff for the wave function and charge density compared to the other phonons. In case of LDA, the low-frequency optical phonons are converged within the error bar of 2–3 cm⁻¹ for a 40 Ry (480 Ry) wave-function (charge-density) cutoff, while in the GGA exceedingly large cutoffs both for the wave function (110 Ry) and charge density (3300 Ry) are needed to obtain the frequencies within the above-mentioned tolerance. Such high cutoffs make the use of the GGA for n LG films for larger n prohibitive computationally. Hence we have used the LDA with a 40 Ry (480 Ry) wave-function (charge-density) cutoff for all the n LG films.

Our calculated Γ point phonon frequencies for graphite and (single-layer) graphene are listed in Table I, together with their symmetry label. For the 12 phonon modes of graphite, these are the labels of the irreducible representation of D_{6h}^4 (its space-group symmetry if we assume that the hexagonal networks of carbon atoms are stacked in the Bernal sequence and the atoms in α and β sites lie in the same plane without any orientational disorder), according to the decomposition²⁷ $D_{6H}^4 = 2(A_{2u} \oplus B_{2g} \oplus E_{1u} \oplus E_{2g})$. The symmetry index also determines which modes are infrared (IR) active and which Raman active, as listed in Table I, according to the decomposition $D_{6H}^4(\text{IR}) = 2(A_{2u} \oplus E_{1u})$ and $D_{6H}^4(\text{Raman}) = 2E_{2g}$. For convenience,²⁶ we denote as “primed” an optical mode in which two atoms in each layer of the graphite unit cell oscillate together in phase but with an opposite phase to the two atoms of the other layers, whereas an unprimed optical mode denotes a case where atoms within the same layer oscillate out of phase with respect to each other.

Our LDA estimates of a_0 and d_0 for the AB -stacked bilayer graphene (2LG) are 2.4394 and 3.3254 Å, respec-

tively. Both of these parameters hardly change with the increasing number of layers in the n LG film. Furthermore, no discernible surface relaxations and reconstructions are found, which needs to be verified experimentally. Ultrathin n LG films also have the stacked honeycomb lattice but with limited number of layers. For AB -stacked n LG films with an even number of layers (EnLG), a center of inversion σ_i exists and hence the symmetry group is D_{3d} . On the other hand, in the case when n is odd (OnLG), the existence of a reflection symmetry σ_h with respect to the middle layer, instead of the center of inversion, gives the symmetry group D_{3h} . We now highlight some interesting aspects of phonons in EnLG (see Table II) and OnLG (see Table III).

At the zone center, the modes $E_{1u}(\text{high})$ and $E_{2g}(\text{high})$ have the same intralayer motion but differ in the relative phase of the carbon displacements in adjacent layers. Consequently, the interlayer interaction in bulk graphite induces a splitting $\Delta(\omega[E_{1u}(\text{high})] - \omega[E_{2g}(\text{high})]) = 7.3$ cm⁻¹ (see Table I). In case of the 2LG film, the above splitting Δ reduces to 4.8 cm⁻¹ (see Table II), indicating a 33% reduction in interlayer interaction in 2LG film with respect to the three-dimensional (3D) graphite. The rigid-layer shear mode $E^*(\text{low})$ in the 2LG film also provides another spectroscopic measure of the interlayer coupling exhibiting the similar 33% reduction in frequency (and hence interlayer bonding) compared to the 3D graphite. In the limit of zero interlayer coupling, one must get $\omega[E_{2g}(\text{low})]$ (and $\omega[B_{2g}(\text{low})]$) $\rightarrow 0$.

More interestingly, the out-of-plane transverse optical phonons $B_{2g}(\text{low})$ and $B_{2g}(\text{high})$, which were optically silent in graphite, become Raman active [$A_{1g}(\text{low})$ and $A_{1g}(\text{high})$, respectively] in the EnLG film. The $A_{1g}(\text{low})$ mode arises while two adjacent layers move out of phase relative to each other (i.e., a “primed” mode mentioned above) along the c axis. In a 2LG film, only one $A_{1g}(\text{low})$ mode is possible, corresponding to $\rightarrow \leftarrow$ vibrational layer displacement along the c axis (which we denote as $+-$ for simplicity). In a 4LG film, two $A_{1g}(\text{low})$ modes are possible, corresponding to $+-+-$ ($\rightarrow \leftarrow \rightarrow \leftarrow$) and $++--$ ($\rightarrow \rightarrow \leftarrow \leftarrow$); in a 6LG film, one gets three $A_{1g}(\text{low})$ modes, corresponding to

TABLE II. Optical (LDA) phonons of even n -layer graphene (EnLG) at the Γ point.

Symmetry	Activity	Frequency (cm ⁻¹)		
		6LG	4LG	2LG
A_{1g}	Raman	25.3	41.6	
E_g	Raman	35.5	37.5	
E_u	IR	39.5		
E_g	Raman	44.8		
E_u	IR	49.5	45.3	
$E_g \Rightarrow E^*(\text{low})$	Raman	53.2	51.4	35.0
A_{2u}	IR	54.9	78.5	
A_{1g}	Raman	79.9		
A_{2u}	IR	96.7		
$A_{1g} \Rightarrow A^*(\text{low})$	Raman	107.8	103.4	76.8
$A_{1g} \Rightarrow A^*(\text{high})$	Raman	894.7	895.2	900.8
A_{2u}	IR	895.5		
A_{1g}	Raman	897.3		
A_{2u}	IR	898.5	897.6	
A_{1g}	Raman	902.2	902.1	
A_{2u}	IR	902.2	902.2	903.3
E_g	Raman	1594.2	1594.2	1594.1
E_u	IR	1594.8	1595.3	
E_g	Raman	1596.1		
E_u	IR	1598.2		
E_g	Raman	1600.2	1598.4	
E_u	IR	1601.3	1601.0	1598.9

$+-+--$, $++--+$, and $+++--$; and in any EnLG film, $n/2$ such modes, corresponding to $n/2$ physically distinct arrangements of the layer displacements, are possible. The counterparts of the above layer displacements in OnLG are the $A_2''(\text{low})$ modes because of σ_h symmetry. Hence they are IR active and not Raman active. Among all the possible combinations, only the $+-+\dots$ up to n ($\leftarrow \leftarrow \leftarrow \dots \leftarrow$ up to n) displacement pattern is omnipresent in all $n(>1)$ -layer graphene and will be denoted as the $A^*(\text{low})$ mode hereafter (see Fig. 1). Particularly in a 3LG film, the A^* mode arises when the outer two layers move in phase and the middle layer moves (with an appropriate amplitude ratio) in the opposite direction (i.e., $\leftarrow \leftarrow \rightarrow$). The counterpart of the $A^*(\text{low})$ phonon in the higher frequency region [denoted as $A^*(\text{high})$ in Tables II and III and Fig. 2] involves relative motion of the intralayer carbon atoms, as mentioned above. The frequency shifts of both $A^*(\text{low})$ and $A^*(\text{high})$ phonons are plotted with respect to the number of layers, respectively, in Figs. 3(a) and 3(b). Figure 3(a) clearly shows that the $A^*(\text{low})$ phonon becomes harder and approaches the frequency value of the $B_{2g}(\text{low})$ mode of graphite with increasing n . This is to be expected because as n increases, the carbon atoms move less freely in the out-of-plane direction compared to a single-layer graphene. In contrast, the $A^*(\text{high})$ phonon softens [as can be seen in Fig. 3(b)], but less dramatically, as n increases, consistent with its atomic-

TABLE III. Optical (LDA) phonons of odd n layer graphene (OnLG) at the Γ point.

Symmetry	Activity	Frequency (cm ⁻¹)		
		7LG	5LG	3LG
A_1'	Raman	24.5	32.1	
E''	Raman	35.0	35.6	
E'	IR+Raman	38.4	42.3	
E''	Raman	42.8		
E'	IR+Raman	47.7		
$E'' \Rightarrow E_1''$	Raman	51.1	48.1	27.6
$E' \Rightarrow E^*(\text{low})$	IR+Raman	53.4	53.0	41.0
A_2''	IR	50.0	67.1	
A_1'	Raman	70.0		
A_2''	IR	90.4		
$A_1' \Rightarrow A_1'$	Raman	102.0	90.6	59.3
$A_2'' \Rightarrow A^*(\text{low})$	IR	108.8	106.8	97.5
$A_2'' \Rightarrow A^*(\text{high})$	IR	894.6	894.9	896.4
A_1'	Raman	895.5		
A_2''	IR	896.9		
A_1'	Raman	898.0	896.6	
A_2''	IR	899.0	898.5	
A_2''	IR	902.2	902.2	902.1
A_1'	Raman	902.3	902.3	902.6
E'	IR+Raman	1594.2	1594.2	1594.1
E''	Raman	1594.6	1594.9	
E'	IR+Raman	1595.6		
E''	Raman	1597.2		
E'	IR+Raman	1599.0	1596.9	
E''	Raman	1600.5	1599.5	1596.0
E'	IR+Raman	1601.4	1601.2	1600.3

displacement pattern. Another low-frequency phonon $E^*(\text{low})$ (see Fig. 4), which has E_g symmetry in EnLG films (and is hence Raman active) and E'' symmetry in OnLG films (and is hence simultaneously Raman and IR active), also shows considerable hardening with increasing n [see Fig. 3(c)]. However, this mode may be difficult to observe in Raman experiments because of its very small frequency value, given the presence of the strong Rayleigh scattering background. In contrast, the $A^*(\text{low})$ phonon, which was silent in bulk graphite, can be used as an unambiguous experimental fingerprint in the n LG film to quantify its interlayer coupling.

To understand how the coupling between the layers changes with the interlayer distance, we also calculate the frequency shifts for bilayer graphene as a function of the percentage contraction of its interlayer separation $[(d_0 - d)/d_0]$. Results for the three phonon modes discussed above, shown in Fig. 3(d), are consistent with the trend obtained with respect to the number of graphene layers.

It is worth drawing attention also to the fact that in an OnLG film, one gets this interesting vibrational mode (such

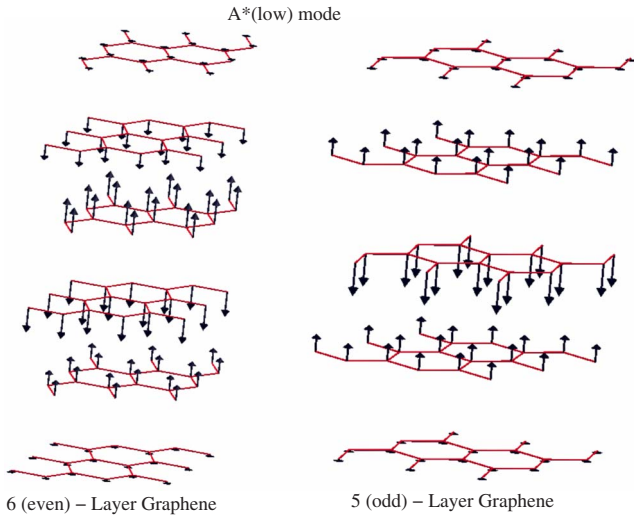


FIG. 1. (Color online) Eigendisplacements of the $A^*(\text{low})$ mode in the AB -stacked six-layer and five-layer graphene films.

as A'_\dagger and E'_\dagger modes) where the atoms in the middle layer do not move at all while the atoms in the outer layers move. These modes, which are not present in an n LG film due to the absence of a single middle layer, can be used to determine the even-oddness of a few-layer graphene film. As can be seen in Table III, the frequencies of the A'_\dagger and E'_\dagger phonons also increase with the number of graphene layers.

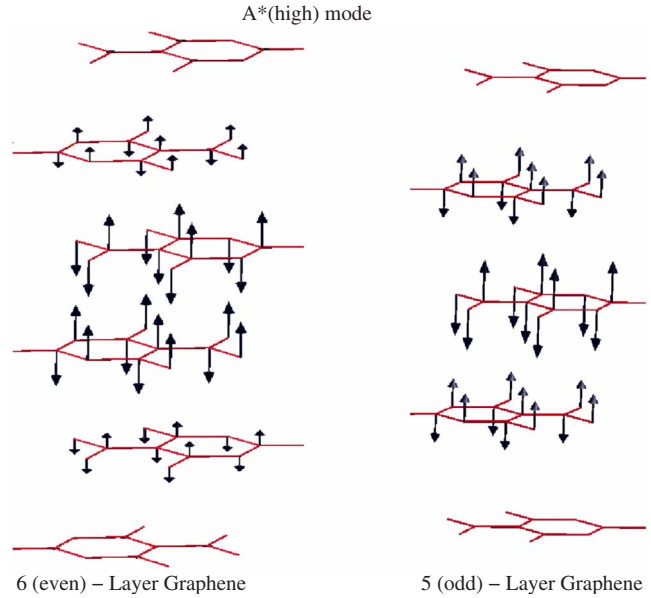


FIG. 2. (Color online) Eigendisplacements of the $A^*(\text{high})$ mode in the AB -stacked six-layer and five-layer graphene films.

In recent Raman experiments,⁶ it has been observed that the frequency of a high-energy optical phonon (Raman G peak at $\sim 1581 \text{ cm}^{-1}$) in n LG films slightly decreases with increasing n . In the lower part of both Tables II and III, there

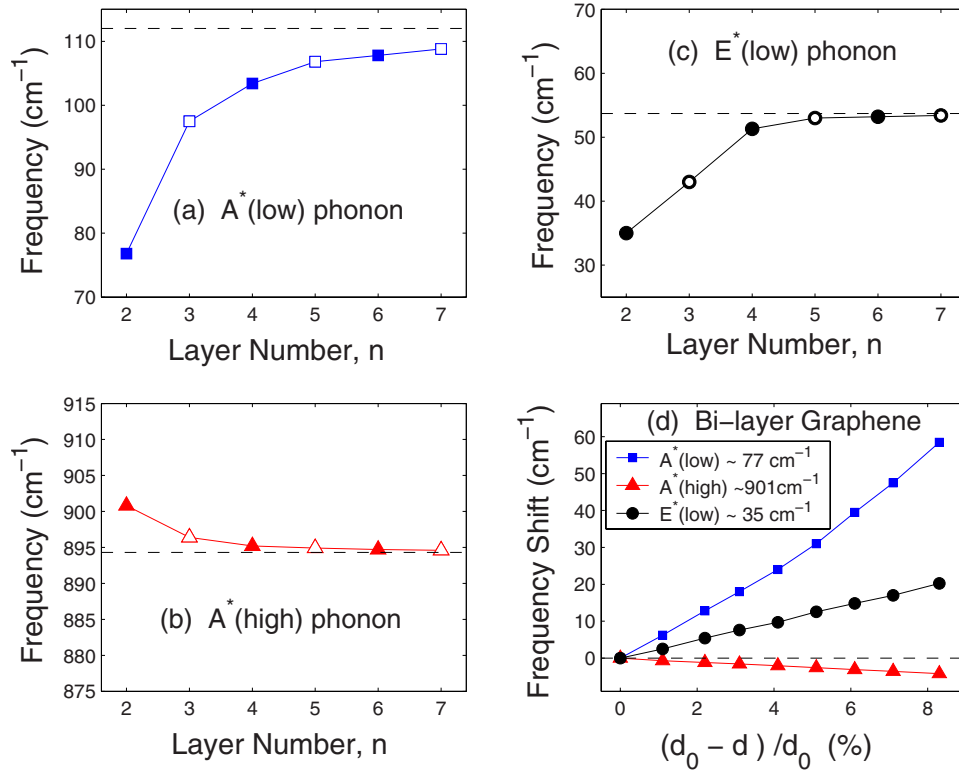


FIG. 3. (Color online) (a) Phonon frequencies of $A^*(\text{low})$ mode in the n LG film as a function of the number of layers n . (b) Those of $A^*(\text{high})$ mode with n . (c) $E^*(\text{low})$ phonon frequencies versus n . (d) Frequency shifts of the above three phonons in bilayer graphene as a function of the percentage contraction of its interlayer separation d_0 . In all figures, solid, open, and thick ring symbols denote, respectively, Raman, IR, and simultaneous Raman and IR activity. In (a)–(c), the dashed lines indicate the corresponding frequency values in bulk graphite.

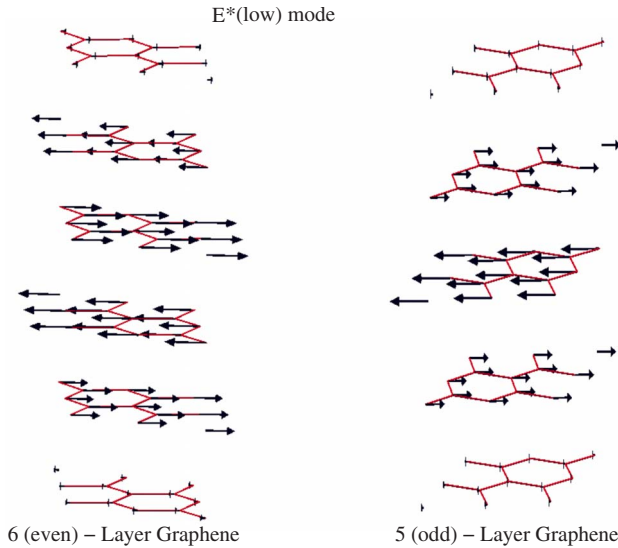


FIG. 4. (Color online) Eigendisplacements of the $E^*(\text{low})$ phonon in the AB -stacked six-layer and five-layer graphene films. For this doubly degenerate mode, we show only one choice; the other eigenvector can be obtained by symmetry.

is evidence for the presence of some sort of frequency shift with respect to the number of graphene layers. However, it is not so simple to compare this shift with the experimentally observed redshifts because of the proximity of many closely spaced phonons and because of the presence of possible unintentional doping in the experiments.

IV. DISCUSSIONS

The most important outcome of this DFT study is the emergence of three zone-center optical phonons, denoted as $E^*(\text{low})$, $A^*(\text{low})$, and $A^*(\text{high})$, which show significantly large sensitivity to the number of layers n . Since no discernible change in the lattice parameter is found as n varies, the obtained shifts in the phonon frequencies can mainly be attributed to the way vibrational motion of a particular mode gets modified when the number of neighboring atoms increases with n . In general, different modes get modified differently as the interplay of the repulsive and attractive forces depends on their characteristic displacement patterns. The $E^*(\text{low})$ mode is a rigid-layer shear mode where adjacent graphene layers slide over each other in oppositely directed motions parallel to the layer planes (see Fig. 4) and its frequency is determined by the interlayer shearing interaction, while the $A^*(\text{low})$ mode is a rigid-layer compressional mode which involves out-of-plane motion (see Fig. 1). Generically, rigid-layer modes involve displacements where whole layers move as single entities and the restoring forces are provided entirely by the interlayer interactions. Both the above interlayer modes harden with increasing n because as n increases (i.e., the coordination gets enhanced) the layers move less freely compared to single-layer graphene. In contrast, the out-of-plane $A^*(\text{high})$ mode which involves displacements,

where atoms within the same layer oscillate out of phase with respect to each other (see Fig. 2), leads to a puckering or distortion of the layer planes and hence is not a rigid-layer mode. This puckering takes advantage of the interlayer coupling in such a way so that atoms can move more easily as the number of layers increases. As a result, the $A^*(\text{high})$ mode shows a dramatically opposite (compared to the above two rigid-layer modes) trend, in that the frequency softens as n increases. Among all, the $A^*(\text{low})$ phonon shows the largest shift in frequency with the number of layers because interlayer bond stretching is most susceptible to the change in the interlayer coupling arising from the change in coordination number (i.e., the number of neighboring atoms).

Finally, we would like to point out that our LDA calculations for the n LG films do not show any noticeable layer reconstructions and relaxations. In view of LDA's known limitations in accounting for interlayer interactions, these findings require experimental verification, which seems not to have been hitherto attempted. A significant rearrangement in n LG films could lead to a C_{3v} symmetry ($A \oplus E_1$) where all the zone-center modes become both IR and Raman active due to lack of an inversion center.³¹ In contrast, AA -stacked n LG films have a D_{6h} symmetry ($A_{1g} \oplus A_{2u} \oplus B_{1u} \oplus B_{2g} \oplus E_{1g} \oplus E_{1u} \oplus E_{2g} \oplus E_{2u}$) irrespective of the evenness or oddness of n . This symmetry includes both the σ_i and σ_h operations, and phonon modes cannot be both Raman and IR active simultaneously. However, the counterparts of A^* mode in those nonideal graphitic materials also exhibit the high sensitivity with respect to the number of layers seen above and hence can be used as experimental fingerprints of their interlayer bindings.

V. CONCLUSION

In conclusion, in this paper we have presented a detailed first-principles analysis of zone-center phonons in n LG films. We have shown that an out-of-plane low-frequency ($\sim 112 \text{ cm}^{-1}$) optical phonon has a particularly large sensitivity to the interlayer binding. Frequency shifts of the out-of-plane phonons in bilayer graphene have also been calculated as a function of the percentage contraction of its interlayer separation. We expect that our calculations will be of value in the context of experimental work, especially in IR and Raman spectroscopies, to develop a better understanding of the interlayer interaction in graphitic materials, which in turn could facilitate the generation of a new exchange-correlation functionals in order to describe this interaction properly.

ACKNOWLEDGMENTS

S.K.S. gratefully acknowledges financial support from the JNCASR. We would also like to acknowledge use of central computing facility from the Centre for Computational Materials Science at JNCASR. A.K.S. and H.R.K. thank the Department of Science and Technology, India for support.

- ¹K. S. Novoselov, A. K. Geim, S. V. Morozov, D. Jiang, Y. Zhang, S. V. Dubonos, I. V. Grigorieva, and A. A. Firsov, *Science* **306**, 666 (2004).
- ²C. L. Lu, C. P. Chang, Y. C. Huang, R. B. Chen, and M. L. Lin, *Phys. Rev. B* **73**, 144427 (2006).
- ³S. Latil and L. Henrard, *Phys. Rev. Lett.* **97**, 036803 (2006).
- ⁴B. Partoens and F. M. Peeters, *Phys. Rev. B* **74**, 075404 (2006).
- ⁵A. C. Ferrari, J. C. Meyer, V. Scardaci, C. Casiraghi, M. Lazzeri, F. Mauri, S. Piscanec, D. Jiang, K. S. Novoselov, S. Roth, and A. K. Geim, *Phys. Rev. Lett.* **97**, 187401 (2006).
- ⁶A. Gupta, G. Chen, P. Joshi, S. Tadigadapa, and P. C. Eklund, *Nano Lett.* **6**, 2267 (2006); Anindya Das, B. Chakraborty, and A. K. Sood, *Bull. Mater. Sci.* **31**, 579 (2008).
- ⁷D. Graf, F. Molitor, K. Ensslin, C. Stampfer, A. Jungen, C. Hierold, and L. Wirtz, *Nano Lett.* **7**, 238 (2007).
- ⁸A. Das, S. Pisana, B. Chakraborty, S. Piscanec, S. K. Saha, U. V. Waghmare, K. S. Novoselov, H. R. Krishnamurthy, A. K. Geim, A. C. Ferrari, and A. K. Sood, *Nat. Nanotechnol.* **3**, 210 (2008).
- ⁹B. Partoens and F. M. Peeters, *Phys. Rev. B* **75**, 193402 (2007).
- ¹⁰S. Latil, V. Meunier, and L. Henrard, *Phys. Rev. B* **76**, 201402(R) (2007).
- ¹¹J. Hass, F. Varchon, J. E. Millán-Otoya, M. Sprinkle, N. Sharma, W. A. de Heer, C. Berger, P. N. First, L. Magaud, and E. H. Conrad, *Phys. Rev. Lett.* **100**, 125504 (2008).
- ¹²M. Aoki and H. Amawashi, *Solid State Commun.* **142**, 123 (2007).
- ¹³Very recently, phonons in multilayered graphene have also been studied but using a multilayer force-constant model by Jin-Wu Jiang, Hui Tang, Bing-Shen Wang, and Zhao-Bin Su, *Phys. Rev. B* **77**, 235421 (2008).
- ¹⁴S. Baroni, S. de Gironcoli, A. Dal Corso, and P. Giannozzi (<http://www.pwscf.org>).
- ¹⁵D. Vanderbilt, *Phys. Rev. B* **41**, 7892 (1990).
- ¹⁶J. P. Perdew and A. Zunger, *Phys. Rev. B* **23**, 5048 (1981).
- ¹⁷J. P. Perdew, K. Burke, and M. Ernzerhof, *Phys. Rev. Lett.* **77**, 3865 (1996).
- ¹⁸H. J. Monkhorst and J. D. Pack, *Phys. Rev. B* **13**, 5188 (1976).
- ¹⁹S. de Gironcoli, *Phys. Rev. B* **51**, 6773 (1995); Srijan Kumar Saha, U. V. Waghmare, H. R. Krishnamurthy, and A. K. Sood, *Phys. Rev. B* **76**, 201404(R) (2007).
- ²⁰<http://www.library.cornell.edu/nr/bookcpdf/c10-7.pdf>
- ²¹S. Baroni, S. de Gironcoli, A. Dal Corso, and P. Giannozzi, *Rev. Mod. Phys.* **73**, 515 (2001).
- ²²D. P. DiVincenzo, E. J. Mele, and N. A. W. Holzwarth, *Phys. Rev. B* **27**, 2458 (1983).
- ²³L. A. Girifalco and M. Hodak, *Phys. Rev. B* **65**, 125404 (2002).
- ²⁴J. C. Charlier, X. Gonze, and J. P. Michenaud, *Phys. Rev. B* **43**, 4579 (1991); *Carbon* **32**, 289 (1994).
- ²⁵N. Ooi, A. Rairkar, and J. B. Adams, *Carbon* **44**, 231 (2006).
- ²⁶N. Mounet and N. Marzari, *Phys. Rev. B* **71**, 205214 (2005).
- ²⁷F. Tuinstra and J. L. Koenig, *J. Chem. Phys.* **53**, 1126 (1970).
- ²⁸R. Nicklow, N. Wakabayashi, and H. G. Smith, *Phys. Rev. B* **5**, 4951 (1972).
- ²⁹P. C. Eklund and J. M. Holden, *Carbon* **33**, 959 (1995).
- ³⁰C. Oshima, *Solid State Commun.* **65**, 1601 (1988).
- ³¹Y. Kawashima and G. Katagiri, *Phys. Rev. B* **59**, 62 (1999).